Simulating the impact of glaciations on continental groundwater flow systems: 1. Relevant processes and model formulation

J.-M. Lemieux,[1] E. A. Sudicky,[1] W. R. Peltier,[2] and L. Tarasov[3]

Received 1 November 2007; revised 9 April 2008; accepted 5 June 2008; published 16 August 2008.

[1] In the recent literature, it has been shown that Pleistocene glaciations had a large impact on North American regional groundwater flow systems. Because of the myriad of complex processes and large spatial scales involved during periods of glaciation, numerical models have become powerful tools to examine how ice sheets control subsurface flow systems. In this paper, the key processes that must be represented in a continental-scale 3-D numerical model of groundwater flow during a glaciation are reviewed, including subglacial infiltration, density-dependent (i.e., high-salinity) groundwater flow, permafrost evolution, isostasy, sea level changes, and ice sheet loading. One-dimensional hydromechanical coupling associated with ice loading and brine generation were included in the numerical model HydroGeoSphere and tested against newly developed exact analytical solutions to verify their implementation. Other processes such as subglacial infiltration, permafrost evolution, and isostasy were explicitly added to HydroGeoSphere. A specified flux constrained by the ice sheet thickness was found to be the most appropriate boundary condition in the subglacial environment. For the permafrost, frozen and unfrozen elements can be selected at every time step with specified hydraulic conductivities. For the isostatic adjustment, the elevations of all the grid nodes in each vertical grid column below the ice sheet are adjusted uniformly to account for the Earth's crust depression and rebound. In a companion paper, the model is applied to the Wisconsinian glaciation over the Canadian landscape in order to illustrate the concepts developed in this paper and to better understand the impact of glaciation on 3-D continental groundwater flow systems.

Citation: Lemieux, J.-M., E. A. Sudicky, W. R. Peltier, and L. Tarasov (2008), Simulating the impact of glaciations on continental groundwater flow systems: 1. Relevant processes and model formulation, *J. Geophys. Res.*, *113*, F03017, doi:10.1029/2007JF000928.

1. Introduction

[2] Continental glaciations that occurred during the Quaternary period had a profound impact on the Canadian landscape. Modifications of continental surface hydrology [e.g., *Teller*, 1990] and surface topography [e.g., *Peltier*, 1994] have been recognized for a long time. Recently, several studies, using environmental isotopes and salinity data, have suggested that significant subglacial meltwater may have infiltrated into the subsurface under the ambient ice sheet pressure and therefore become stored in the groundwater flow system (e.g., *Clark et al.* [2000], *Douglas et al.* [2000], *Grasby et al.* [2000], *Edmunds* [2001], *Ferguson et al.* [2007], and *Person et al.* [2007] among others). Geochemical studies have provided compeling evidence of glacial meltwater recharge in the Canadian Shield [*Raven et al.*, 1987], in the North Central United States [*Siegel and Mandle*, 1983; *Siegel*, 1989, 1991; *McIntosh et al.*, 2002; *McIntosh and Walter*, 2005], Western Ontario [*Weaver et al.*, 1995] and in the Western Canada sedimentary Basin [*Grasby and Chen*, 2005]. Because of the small pore spaces within the underlying rocks, a relatively small quantity of recharge into the subsurface can considerably raise pore pressures and therefore modify the groundwater flow field.

[3] Pressurized groundwater below ice sheets may also be an important consideration with regard to issues such as the safe long-term disposal of radioactive wastes [*Sheppard et al.*, 1995; *Talbot*, 1999; *Heathcote and Michie*, 2004]. Because the suitability of deep geologic repositories must be demonstrated over large timescales, flow patterns under an ice sheet must be understood as they may change drastically.

[4] Many processes affect the evolution of groundwater flow systems during a glacial cycle and these processes are typically strongly coupled. As such, numerical models have become powerful tools to study the impact of glaciation on groundwater flow dynamics over large time frames. In the recent literature, several authors have presented results from numerical modeling studies on the effects of glaciation on

[1]Department of Earth and Environmental Sciences, University of Waterloo, Waterloo, Ontario, Canada.
[2]Department of Physics, University of Toronto, Toronto, Ontario, Canada.
[3]Department of Physics and Physical Oceanography, Memorial University, St. John's, Newfoundland & Labrador, Canada.

0148-0227/08/2007JF000928

groundwater flow. The approaches taken are diverse, but all large-scale studies have ignored important factors known to influence groundwater flow patterns. For instance, several of them were performed as a series of steady state time slices [*Boulton et al.*, 1993, 1995, 1996; *Piotrowski*, 1997a, 1997b; *van Weert et al.*, 1997; *Breemer et al.*, 2002; *Hoaglund et al.*, 2004]. A glaciation is a highly transient event and groundwater pressure evolves slowly. Subsurface pressure distributions are likely to be significantly influenced by historical conditions because of the long time needed for water to flow in low-permeability rocks, especially at depth. This was recognized by *Provost et al.* [1998], *Person et al.* [2003, 2007], *McIntosh et al.* [2005], and V. F. Bense and M. A. Person (Transient hydrodynamics within inter-cratonic sedimentary basins during glacial cycles, submitted to *Journal of Geophysical Research*, 2008) who performed transient analysis along 2-D cross sections. Detailed 3-D analysis was performed by *Chan et al.* [2005] and *Chan and Stanchell* [2005] at the site scale in the context of the Benchmark Test 3 of the international DECOVALEX III (Development of Coupled Thermo-hydro-mechanical Models and Their Validation Against Experiments in Nuclear Waste Isolation) project and a detailed 2-D subglacial hydrology model that couples glacier surface runoff, englacial water storage and transport, subglacial drainage, and subsurface groundwater flow was presented by *Flowers and Clarke* [2002a, 2002b] and applied at the catchment scale.

[5] The objectives of this paper are to review the processes that are relevant to include in a 3-D numerical model to simulate the impact of glaciations on groundwater flow systems at the scale of the basin and continent and to demonstrate how these processes can be both simplified and accurately included in a numerical model to allow time efficient simulations of groundwater flow and solute transport. The model has already been successfully applied for the analysis of recharge and seepage patterns (i.e., fluxes across the ground surface) over the Canadian landscape during the Wisconsinian glaciation [*Lemieux et al.*, 2008a], but only a brief description of the numerical model was given. In this paper, an extensive description of the model is performed and a set of exact analytical solutions are developed to verify the implementation of hydromechanical loading and brine generation. The use of a simple analytical solution also provides insights into these complex processes that are challenging to capture when they are all acting together.

[6] In a companion paper [*Lemieux et al.*, 2008b], the model is applied to the Wisconsinian glaciation over the Canadian landscape in order to illustrate the concepts developed in this paper and to better understand the impact of glaciations on continental groundwater flow up to a depth of 10 km in the Earth crust.

2. Hydraulic Conditions During a Glacial Cycle

[7] Hydraulic conditions during a glacial cycle are different than currently observed in some notable ways (see *Lemieux et al.* [2008a] for a detailed review of their evolution during a glacial cycle) and are in direct relation with the climatic conditions during the Ice Age, from which the major component is the continental flowing ice sheet and coevolution of permafrost. Figure 1 exhibits a summary of the hydraulic conditions during a glaciation period along a schematic cross section.

[8] The permeability of soils affected by permafrost is greatly reduced [*Burt and Williams*, 1976] such that extensive permafrost prevents surface water from recharging groundwater and conversely from allowing groundwater to discharge to the surficial regime [*McEwen and de Marsily*, 1991]. Although the term "permafrost" is commonly used in the context of frozen soils and rocks, there are different types of permafrost and each will have a different impact on groundwater flow. Continuous permafrost is usually referred to as a material in which all of the water within the soil is permanently frozen. Discontinuous permafrost represents a large body of permafrost that contains some unfrozen sections. Sporadic permafrost is found in isolated, small patches of permanently frozen ground, and intermittent permafrost refers to soil/rock freezing conditions that can change from year to year. In regions of discontinuous and sporadic permafrost, surface water and groundwater can interact through the unfrozen sections. Structures such as talik, which are "holes" of unfrozen ground, have been observed below large surface water bodies even in regions where the permafrost is quite deep in the surroundings. These taliks can allow recharge or discharge of deep groundwater [*McEwen and de Marsily*, 1991]. Figure 2 shows the current permafrost distribution across Canada as well as permafrost thicknesses. Clearly, the impact of permafrost zones will have a large effect on regional groundwater flow patterns, and therefore must be included in a continental-scale groundwater flow model intended to capture the effects of the advance and retreat of ice sheets over a glacial cycle.

[9] The weight of the ice sheet will cause the Earth's crust to deform. The deformation of the crust by the ice sheet is such that the Earth's surface elevation will be depressed below the ice sheet (isostatic depression) and raised in its far surroundings. The stress conditions under the ice sheet will be compressive, while horizontal tensile stresses will affect the forebulge [*Ates et al.*, 1997]. This will modify large-scale groundwater flow patterns because hydraulic potentials will be lowered below the ice sheet and increased in the forebulge. Another impact of the ice sheet is the additional weight imposed on the geologic medium. Depending on the elastic properties of the medium, which are a function of the rock type, compaction can reduce both the porosity and the hydraulic conductivity and increase the pore pressure.

[10] Subglacial meltwater generated because of ice sheet basal friction and the Earth's geothermal gradient will be either driven into the subsurface under ice sheet pressure or will flow toward ice sheet margin through a series of conduits.

[11] The regressions of the ice and its weight allows the compacted rock to expand toward its initial state. Groundwater that was under ice sheet pressure and flowing downward from the surface therefore reverses its flow direction and can now migrate upward toward the land surface. This behavior is well documented in the Michigan Basin [*McIntosh and Walter*, 2005] and the Williston Basin [*Grasby et al.*, 2000]. Proglacial lakes formed at the ice

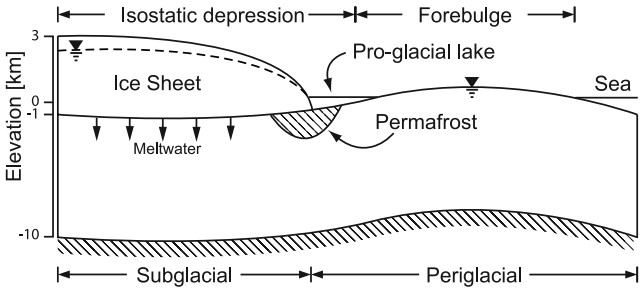

Figure 1. Cross section along an ice flow line showing hydraulic conditions during a glacial cycle. Extent of the subglacial and periglacial environments is also shown.

margins in the isostatic depressions. The depth of the depressions evolves as the Earth's crust recovers to its initial state. The proglacial lakes stage, depth and extent was a result of the interactions among the location of the ice margin, the topography of the newly deglaciated surface, the elevation of the active outlet, and differential isostatic rebound [*Teller*, 1987]. Finally, the dynamic eustatic sea level due to water storage into ice sheets constantly modifies the sea shore position and coastal water levels.

3. Numerical Model

[12] The linkage of climate models to groundwater flow models is usually performed by an asynchronous forcing of the groundwater flow model with the results of a climate model, usually a global circulation model [e.g., *Brouyère et al.*, 2004]. The approach used in this study is similar, but the complexity arising from the glacial component of the climate model raises the need to include a more complex set of boundary conditions not commonly used in conventional groundwater flow modeling studies. We include other important factors such as the influence of permafrost development/thawing, changing topography due to isostasy, sea level change on coastal margins due to ice sheet formation/thawing and the presence of high-salinity paleobrines at depth in the continental interior.

3.1. Ice and Climate Model

[13] The inferred ice and climate chronologies during the Wisconsinian glaciation presented here are derived from the Memorial University of Newfoundland/University of

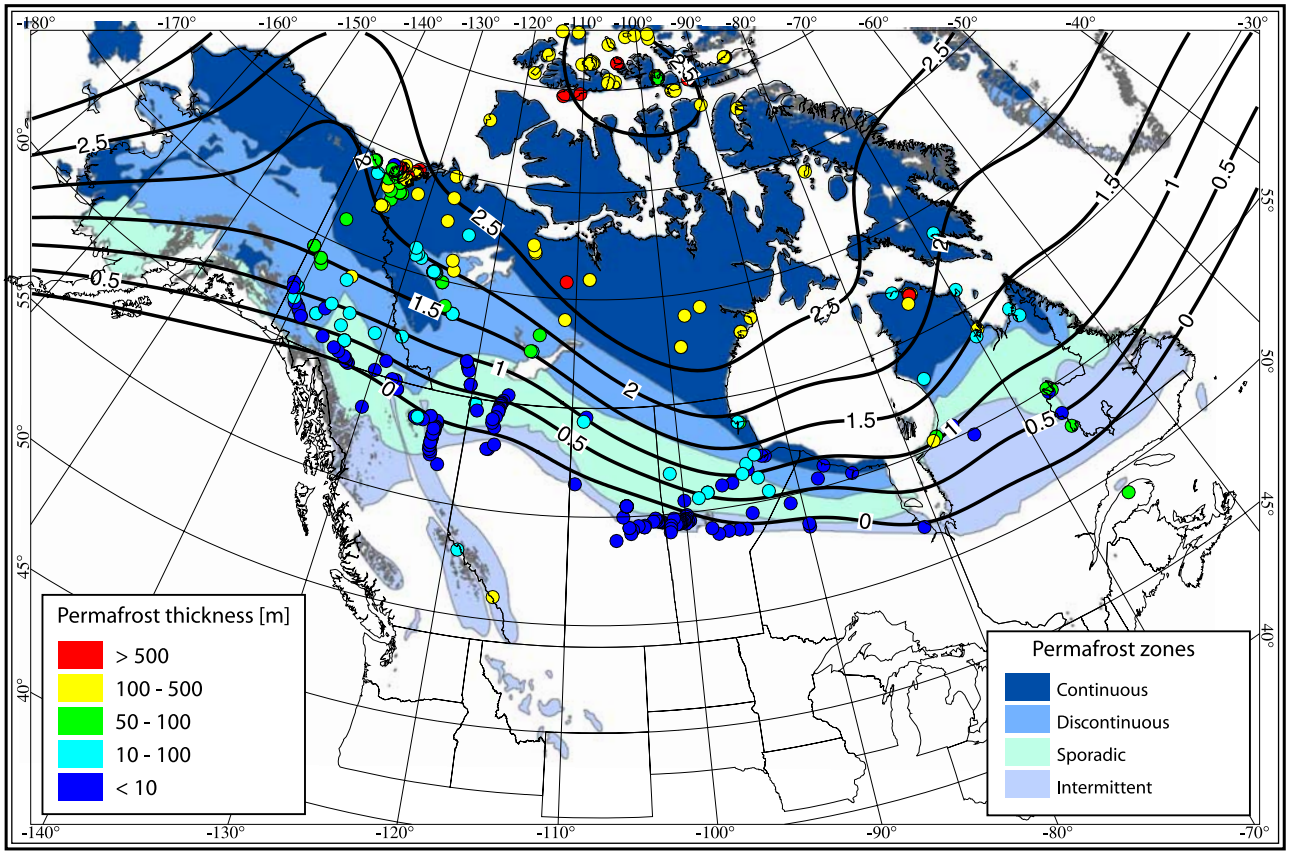

Figure 2. Permafrost distribution at present time. Permafrost extent is shown on a contoured blue scale. The permafrost can be continuous, discontinuous, sporadic, or intermittent. The depth of the zero degree isotherm, referred as the permafrost thickness, is shown as scatter points with a rainbow color scale. The bold black contours represent the permafrost thickness interpolation of the scatter points displayed on a $\log_{10}$ scale. Sources are *Smith and Burgess* [2002] for the permafrost thickness database and *International Permafrost Association Standing Committee on Data Information and Communication* [2003] for the permafrost distribution.

Toronto Glacial Systems Model (GSM). The GSM is composed of eight components linked together and representing, respectively, surface mass balance, thermomechanically-coupled ice sheet dynamics [*Tarasov and Peltier*, 1999, 2002], bed thermodynamics, basal dynamics, ice calving, isostasy, surface drainage [*Tarasov and Peltier*, 2006], and climate forcing [*Tarasov and Peltier*, 2004]. Details of the model are given by *Lemieux et al.* [2008a].

[14] The GSM was executed over the past 120 ka on a 1.0° longitude by 0.5° latitude grid resolution in order to produce a data set for surface elevation, ice sheet thickness, relative sea level, permafrost thickness and subglacial melting rate.

3.2. Groundwater Flow Model

[15] The model used for this work is HydroGeoSphere [*Therrien et al.*, 2006] which is an extended version of the FRAC3DVS code [*Therrien and Sudicky*, 1996]. HydroGeoSphere is a three-dimensional control volume finite element numerical model describing fully integrated subsurface and surface flow. It also solves for the advective-dispersive transport of solutes both in the surface and the subsurface and the Picard iteration algorithm is used to solve the density-dependant nonlinear flow equation. In this study, the surface component of the model was not used and therefore will not be described. The governing equations of HydroGeoSphere as well as additions concerning 1-D hydromechanical coupling and brine generation are presented in this section.

3.2.1. Darcy Equation

[16] The Darcy equation describing density-dependant subsurface flow in HydroGeoSphere is given by [*Frind*, 1982; *Graf*, 2005]

$$q_i = -K_{ij}\frac{\mu_0}{\mu(T,c)}\left(\frac{\partial h^*}{\partial x_j}+\rho_r\frac{\partial z}{\partial x_j}\right) \quad i,j=1,2,3, \tag{1}$$

where q_i is the Darcy flux (L T^{-1}), K_{ij} is the hydraulic conductivity tensor (L T^{-1}), μ_0 is the reference viscosity (M L^{-1} T^{-1}), $\mu(T, c)$ is the actual fluid viscosity (M L^{-1} T^{-1}) as a function of the fluid temperature and fluid composition (i.e., concentration, c) and h^* is the equivalent freshwater head (L) defined by *Frind* [1982] as

$$h^* = \frac{p}{\rho_0 g}+z, \tag{2}$$

where ρ_0 is the reference density (M L^{-3}), or density of freshwater, p is fluid pressure (M T^{-2} L^{-1}), g is gravitational acceleration (L T^{-2}) and z is elevation above the datum (L). In equation (1), ρ_r is the relative density (M L^{-3}) given by

$$\rho_r = \frac{\rho}{\rho_0}-1, \tag{3}$$

where ρ is the actual density of the fluid.

[17] The hydraulic conductivity tensor is defined as

$$K_{ij} = \frac{k_{ij}\rho_0 g}{\mu(T,c)} \qquad i,j=1,2,3, \tag{4}$$

where k_{ij} is the permeability tensor (L^2). From equation (1), it can be seen that the Darcy flux is a function of both the hydraulic gradient and the buoyancy forces because of the relative density ρ_r. It should be noted that the buoyancy term $\rho_r \partial z/\partial x_j$ acts such that dense brines will tend to migrate vertically downward, or maintain their preexisting distribution at depth, whereas the low total dissolved solids (TDS), low-density water infiltrating as glacial meltwater will be constrained to occur at shallow depths. Dispersive mixing processes will, however, create a transition zone between the fresh and brine water regimes. A description of this transition zone requires a solution to the coupled advection-dispersion equation which is described later.

3.2.2. Fluid Continuity Equation

[18] The three-dimensional fluid continuity equation for transient density and viscosity-dependant groundwater flow expressed in terms of an equivalent freshwater head is given by [*Frind*, 1982; *Graf*, 2005]

$$\frac{\partial}{\partial x_i}\left[K_{ij}\frac{\mu_0}{\mu}\left(\frac{\partial h^*}{\partial x_j}+\rho_r\frac{\partial z}{\partial x_j}\right)\right] = S_s\frac{\partial h^*}{\partial t} \qquad i,j=1,2,3, \tag{5}$$

where S_S is specific storage (L^{-1}) defined as [*Freeze and Cherry*, 1979]

$$S_S = \left(\beta_{pm}+\phi\beta_f\right)\rho_0 g, \tag{6}$$

where β_{pm} and β_f are, respectively, the aquifer and water compressibility (L T^2 M^{-1}) and ϕ is the porous medium's porosity (dimensionless). Equation (5) together with equation (6) is the standard equation describing groundwater flow in a nondeformable geologic material; however, because of glacial loading and unloading, consideration must be given to the impact of rock deformation on fluid flow.

[19] *Wang* [2000] and *Neuzil* [2003] showed that the assumption of purely vertical strain can be used to describe flow in two- and three-dimensional regimes with small resulting errors provided that only homogeneous and laterally extensive overburden changes occur. In such cases, equation (5) becomes

$$\frac{\partial}{\partial x_i}\left[K_{ij}\frac{\mu_0}{\mu}\left(\frac{\partial h^*}{\partial x_j}+\rho_r\frac{\partial z}{\partial x_j}\right)\right] = S_s\frac{\partial h^*}{\partial t}-S_s\zeta\frac{1}{\rho g}\frac{\partial \sigma_{zz}}{\partial t}, \quad i,j=1,2,3, \tag{7}$$

where σ_{zz} is the vertical stress (M T^{-2} L^{-1}) and where ζ is the one-dimensional loading efficiency (dimensionless) given by

$$\zeta = \frac{\beta_{pm}}{\beta_{pm}+\phi\beta_f}, \tag{8}$$

with the assumption of incompressible grains [*Lemieux*, 2006]. The loading efficiency varies between 0 and 1 and specifies how much of the surface loading is transferred to the subsurface fluid.

[20] Equation (7) alone provides a complete description of transient flow in the presence of vertical stress changes. To account for the change in overburden load with time, $\partial\sigma_{zz}/\partial t$ must be specified, which can be obtained from ice thickness evolution.

3.2.3. Solute Continuity Equation

[21] The three-dimensional solute continuity equation for a conservative solute is given by

$$\frac{\partial}{\partial x_i}\left(\phi D_{ij}\frac{\partial c}{\partial x_j} - q_i c\right) + \Gamma_{1st} = \frac{\partial(\phi c)}{\partial t} \quad i,j = 1,2,3, \tag{9}$$

where c is the solute concentration (M L^{-3}) and Γ_{1st} is a first-order source term (M T^{-1} L^{-3}). The hydrodynamic dispersion coefficient, which accounts for mechanical dispersion and molecular diffusion, is given by [*Bear*, 1972]

$$\phi D_{ij} = (\alpha_l - \alpha_t)\frac{q_i q_j}{|q|} + \alpha_t |q|\delta_{ij} + \phi\tau D^*\delta_{ij}, \tag{10}$$

where α_l and α_t are the longitudinal and the transverse dispersivities (L), $|q|$ is the magnitude of the Darcy flux (L T^{-1}), τ is the matrix tortuosity (dimensionless), D^* is the solute free diffusion coefficient (L^2 T^{-1}), and δ_{ij} is the Kronecker delta which is equal to one when $i = j$ and zero when $i \neq j$. The product τD^* represents an effective diffusion coefficient for the matrix (L^2 T^{-1}). In equation (9), the assumption of fluid incompressibility is made.

[22] The concentration variable is linked to the fluid density with the following linear relationship:

$$\rho_r = \gamma\frac{c}{c_{\max}}, \tag{11}$$

where $c_{\max}$ is the maximum fluid concentration (M L^{-3}) and the dimensionless constant γ is the maximum relative density (dimensionless) given by

$$\gamma = \frac{\rho_{\max}}{\rho_0} - 1, \tag{12}$$

where the assumption is made that the relative solute concentration of a fluid with the density $\rho = \rho_{\max}$ is $c/c_{\max} = 1$. Because of the dependence of fluid flow (equation (7)) and parameters appearing in it on the fluid density and viscosity, it is necessary to couple the flow equation (7), expressed here in terms of equivalent freshwater heads, and the solute transport equation (9) because of the interactions involved. In HydroGeoSphere, the two nonlinear equations are solved via Picard iteration at each time step.

[23] Although water viscosity in brines is known to be a function of solute concentration [e.g., *Adams and Bachu*, 2002], a constant viscosity was used in the simulations. The use of a constant viscosity is a simplification that was necessary to reduce the nonlinearity in the coupled groundwater flow and solute transport equations.

[24] In order to represent brine formation, a process that depends in the difference of concentration between TDS in the fluid and a potential maximum concentration generated by rock weathering, leaching of saline fluid inclusions or other processes is used. A first-order source term (M T^{-1} L^{-3}), Γ_{1st}, is defined as

$$\Gamma_{1st} = k_{mt}(c_{\max} - c), \tag{13}$$

where k_{mt} is a mass transfer coefficient rate (T^{-1}) describing rock water mass interactions and $c_{\max}$ is the maximum allowable fluid concentration (M L^{-3}). The maximum allowable fluid concentration, $c_{\max}$, could represent the saturation concentration of TDS in the case of rock weathering or the concentration of TDS in fluid inclusion, in the case of leaching [*Provost et al.*, 1998].

[25] As *Provost et al.* [1998] point out, this simple expression for the formation of brine captures two basic features of rock water interactions: the rate at which the solids dissolve diminishes as the concentration of the resident fluid increases, and dissolution ceases when the maximum concentration is reached. This approach has the advantage of its simple formulation and because it is a first-order approximation to Fick's law of diffusion that describes mass transfer between mobile and immobile fluid zones.

3.2.4. Energy Transport

[26] While groundwater flow models with energy transport and water-ice phase change has been developed [e.g., *McKenzie et al.*, 2007; Bense and Person, submitted manuscript, 2008], the computational burden for such a task, at our model scale, was considered prohibitive. Although water viscosity and density are expected to be affected by temperature, we believe that the most important impact of temperature is on permafrost development, which is obtained from the GSM. Therefore, viscosity and density are not taken to evolve with temperature, and density is considered to only be a function of TDS concentration, while viscosity is held constant for numerical reasons. We recognize that a more accurate distribution of permafrost could be obtained from a 3-D subsurface energy transport and water-ice phase model, and that a more accurate calculation of hydraulic heads could have been obtained with a viscosity/density evolution with temperature, but because of the exploratory nature of this study, these simplifications were considered appropriate. Permafrost handling in the numerical model is described in a later section.

4. Verification Tests

[27] In this section, the implementation of 1-D hydromechanical coupling and brine generation in the HydroGeoSphere code is verified by comparison to exact analytical solutions. Because previously published solutions are unknown, simple 1-D analytical solutions were specifically developed for each case. Along with verifying the code, the analytical solutions provide an efficient basis to grasp the basic impacts of select processes on flow and solute transport.

4.1. One-Dimensional Hydromechanical Coupling

[28] A 1-D vertical column of sand is shown in Figure 3. The column has a semi-infinite length and is fully saturated. A mass (or load) M is added at the inlet at constant intervals such that dM/dt is a constant. M can be converted to an equivalent water height using the density of water and could represent an ice sheet forming above an aquifer, for example. The top of the column is drained and the bottom is a no-flow boundary condition.

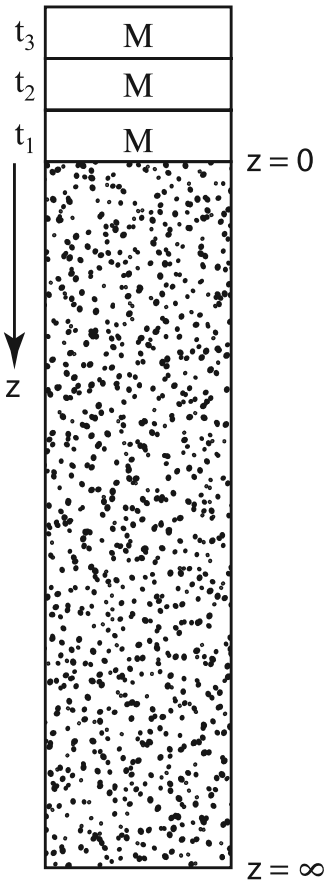

Figure 3. One-dimensional soil column.

4.1.1. Analytic Solution

[29] The governing equation describing flow along the column with mechanical loading is a simplification along the vertical dimension of equation (7). It is given by

$$D\frac{\partial^2 h}{\partial z^2} - \frac{\partial h}{\partial t} + \frac{q_{in}}{S_s} = 0, \tag{14}$$

where $D = K_{zz}/S_s$ is hydraulic diffusivity and

$$q_{in} = S_s \zeta \frac{\partial(\sigma_{zz}/\rho g)}{\partial t} \tag{15}$$

is the source term due to external loading. The initial and boundary conditions are given by

$$\text{I.C.}: \quad h(z, t = 0) = 0, \tag{16}$$

$$\text{B.C.1}: \quad h(z = 0, t) = 0, \tag{17}$$

$$\text{B.C.2}: \quad \frac{\partial h(z = \infty, t)}{\partial z} = 0. \tag{18}$$

[30] Equation (14) is a second-order nonhomogeneous partial differential equation (PDE) that can be solved with integral transforms. Applying the Laplace transform to equation (14) yields

$$\frac{d^2\bar{h}}{dz^2} - \frac{p\bar{h}}{D} + \frac{q_{in}}{DS_s}\frac{1}{p} = 0, \tag{19}$$

where $\bar{h}$ is the Laplace transformation of h, defined as

$$\bar{h}(x, p) = \int_0^\infty \exp(-pt)h(x, t)dt. \tag{20}$$

[31] Equation (19) is a second-order nonhomogeneous ordinary differential equation (ODE) with the following solution:

$$\bar{h} = A\exp\left(z\sqrt{p/D}\right) + B\exp\left(-z\sqrt{p/D}\right) + \frac{q_{in}}{S_s p^2}, \tag{21}$$

where A and B are constants of integration. The constant A is found to be null when using the second boundary condition (equation (18)). The first boundary condition (equation (17)) is used to solve for the constant B

$$B = -\frac{q_{in}}{S_s p^2}. \tag{22}$$

The solution for equation (19) is therefore

$$\bar{h} = \frac{q_{in}}{S_s p^2} - \frac{q_{in}}{S_s p^2}\exp\left(z\sqrt{p/D}\right). \tag{23}$$

[32] It is possible to invert this solution from Laplace space to real-time space using tables from [*Carslaw and Jaeger*, 1959]. The solution for the hydraulic head along the column is

$$h(z, t) = \frac{\zeta}{\rho g}\frac{\partial \sigma_{zz}}{\partial t}\left[t - \left(t + \frac{z^2}{2D}\right)\text{erfc}\left(\frac{z}{2\sqrt{Dt}}\right)\right] - z\sqrt{\frac{t}{\pi D}}\exp\left(-\frac{z^2}{4Dt}\right). \tag{24}$$

4.1.2. Numerical Solution

[33] The physical system described above is modeled using HydroGeoSphere. The analytical solution was developed for a semi-infinite domain and, therefore, to compare the numerical solution with the analytical solution, a domain of 10,000 m length was used. The system represents a 1-D vertical column of length 10,000 m on to which an ice sheet is taken to grow in thickness at a rate of 0.32 meters of ice per year, which is equivalent to 0.3 meters of water equivalent loading per year for 10 ka. The top of the column is drained and as such a specified head of 0.0 m was assigned in the model. The initial head along the length of the column is set to 0.0 m. The properties of the rock mass are described in Table 1. A loading efficiency of unity was used in this "base case" scenario.

[34] Figure 4 shows the hydraulic head versus time at different depths in the column. It can be seen that the numerical solution precisely corresponds to the analytical solution results. It can also be seen that after 10 ka, the head at at a depth of 500 m reaches a value of about 500 m.

Table 1. Material Properties

Properties	Value
K_{zz} (m/a)	1.0×10^{-3}
S_s (m^{-1})	1.0×10^{-6}
ζ	1.0

Figure 5 shows vertical profiles of heads along the column at various times. Again, the numerical solution fits the analytical solution very well. It also indicates that the head along the column increases with depth, noting that the low head value near the surface is due to the specified head boundary condition. It is clear that the impact of the ice sheet loading occurs along the entire vertical length of the column given that the initial head was 0.0 m along its length. The maximum head equals about 925 m at a depth of 1000 m after 10 ka.

[35] The analytical solution was further explored to capture the sensitivity of the values of the loading efficiency on the solution. Figure 6 shows the head solution along the column after 10 ka using different values of the loading efficiency parameter as input. It can be seen that the load transfer to fluid pressure is maximum when the loading efficiency is maximum. As the loading efficiency diminishes, the maximum head becomes lower since more of the externally-applied load is supported by the matrix.

[36] The primary effect of surface loading is to decrease the porespace, which in turn increases the pore pressure. If the loading occurs on a surface and the water is allowed to drain out of the soil, the consequence of the surface loading will be groundwater exfiltration on the surface because the hydraulic head in the subsurface will become higher than that of the surface. On the other hand, if a specified head is applied on the surface along with surface loading, there will be infiltration into the subsurface as long as the head on the surface is higher than in the subsurface, which would occur for loading efficiency values below 1.0. During unloading, the opposite would happen; if the top of the column is drained, water would infiltrate into the subsurface to fill the porespaces that are inflating because of surface unloading. In the case of a surface specified head, exfiltration would occur during unloading because the head in the subsurface would be higher than that at the surface because large infiltration would have occurred earlier and raised the hydraulic head at depth.

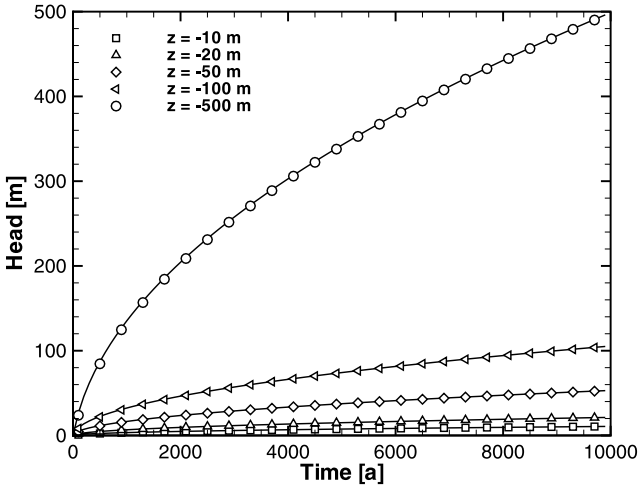

Figure 4. Hydraulic head versus time at different depths along the column. Solid lines represent analytical solution, and symbols represent the numerical solution.

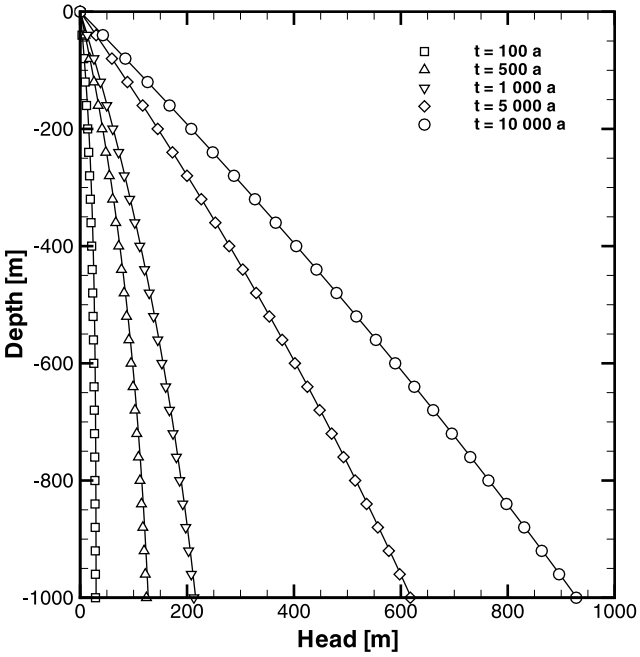

Figure 5. Hydraulic head versus depth at different times. Solid lines represent analytical solution, and symbols represent the numerical solution.

[37] To explore this behavior, the boundary condition at the surface of the column was altered in order to study its impact on the surface/subsurface water interaction at the ice sheet sole. The simulation of the 1-D column was extended for 20 ka over which, during the first 10 ka, a loading rate identical to the base case was applied. During the remaining

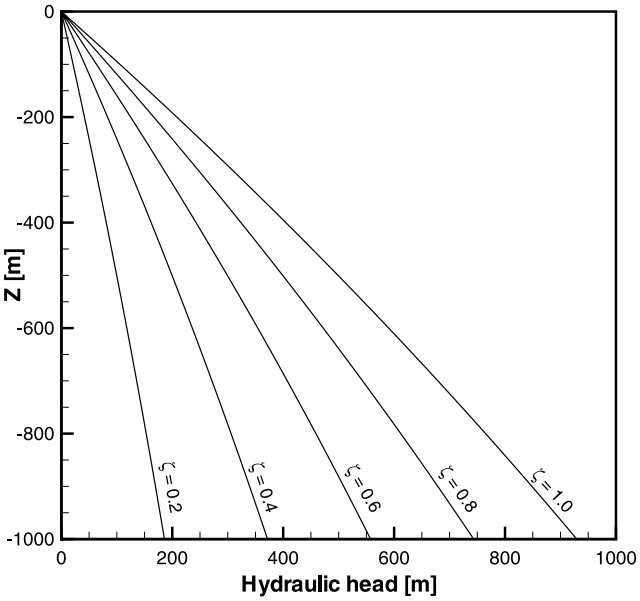

Figure 6. Hydraulic head versus depth for different loading efficiency values.

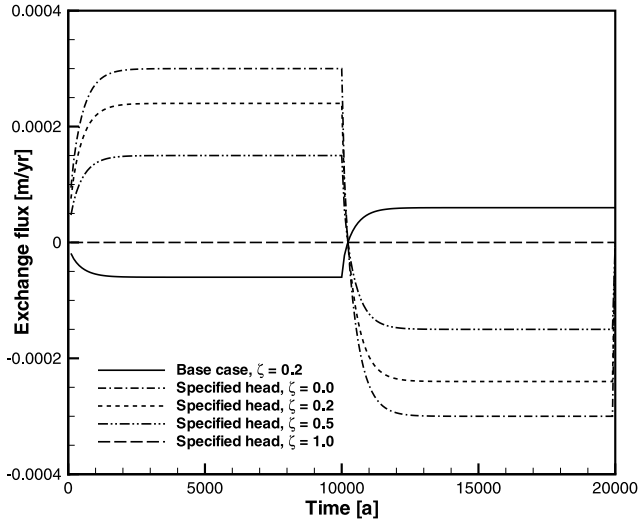

Figure 7. Exchange flux at the top of the column for different scenarios.

10 ka, the ice sheet was assumed to melt at the same rate. The loading efficiency is set to 0.2 and values will be modified from this value to capture its impact on surface/subsurface water interactions.

[38] Figure 7 illustrates the surficial exchange flux for the base case scenario over the duration of the simulation period. It can be seen that, as expected, if the top of the column is drained, water can exfiltrate from the subsurface to the surface during ice sheet buildup because of porespace reduction. During the melting period (10–20 ka), water infiltrates into the subsurface to fill the inflating pore space.

[39] The base case scenario is now modified using a specified head equal to the ice sheet equivalent freshwater head applied on the surface. The surface head will vary linearly from 0 m at the beginning of the simulation to 3000 m at 10 ka and reverts back to 0 m at the end of the simulation, at 20 ka. It can be seen from Figure 7 that the exchange flux is reversed from the base case; during the first 10 ka, water infiltrates into the subsurface because the head at the surface is higher than the values just into the subsurface. During ice sheet melting, the water exfiltrates on the surface because the hydraulic gradient is reversed. The magnitude of the water exchange flux at the surface is clearly dependent on the value of the loading efficiency as can be seen in Figure 7. The loading efficiency parameter was varied from the base case value and it can be seen that the exchange flux is maximum when $\zeta = 0.0$ and null when $\zeta = 1.0$. The exchange flux is null when $\zeta = 1.0$ because all the weight of the ice sheet is transferred to the fluid so there is no hydraulic gradient between the surface and the subsurface. The surface/subsurface water interaction dynamics are therefore a function of the interaction between the subglacial boundary conditions and the elastic properties of the rocks.

4.2. Brine Formation

[40] In order to verify the implementation of the first-order source term in HydroGeoSphere, an analytical solution is derived for the case of steady state flow along a horizontal column. The 1 m long column is open at both ends and a Type III (i.e., Cauchy) boundary condition is specified at the inlet and a free exit boundary condition at the outlet. Mass is produced inside the column at a first-order rate, k_{mt}, of 86.4 d^{-1}. The porous medium is a well-sorted sand in which a constant average linear groundwater velocity of 1.0 m/d is specified. The longitudinal dispersion coefficient is 0.1 m, the diffusion coefficient of the solute is zero and the porosity of the sand, ϕ, equals 0.3. The initial concentration is zero and the maximum concentration is 0.3.

[41] The one-dimensional governing equation describing the transport of a conservative solute is

$$\frac{\partial C}{\partial t} = -v\frac{\partial C}{\partial x} + \alpha_l v\frac{\partial^2 C}{\partial x^2} + \frac{k_{mt}}{\phi}(C_{\max} - C). \tag{25}$$

The boundary conditions for equation (25) are a third type Cauchy at the inlet ($x = 0$) and a zero dispersive flux at $x = L$

$$vc(0,t) - \alpha_L v\frac{\partial c(0,t)}{\partial x} = 0, \tag{26}$$

$$\frac{\partial c(L,t)}{\partial x} = 0, \tag{27}$$

$$c(x,0) = 0. \tag{28}$$

Equation (25) was solved using Laplace transforms in conjunction with the commercial package Maple. The solution in Laplace space is complex and its inversion was performed numerically using *de Hoog et al.*'s [1982] algorithm.

[42] The analytical solution results at the outlet are shown in Figure 8 along with the numerical solution and it can be seen that the match is very good. The concentration rises

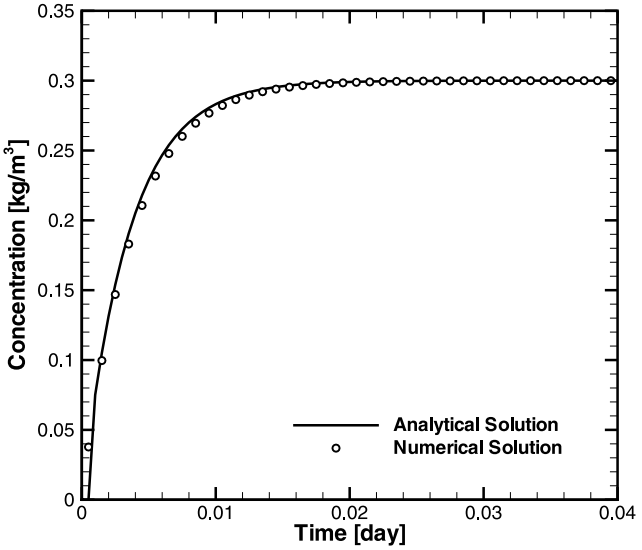

Figure 8. Concentration versus time at the column outlet.

quickly at the beginning and rapidly reaches the maximum fluid concentration of 0.3.

5. Other Relevant Processes

[43] In the previous sections, processes described by differential equations were presented along with their implementation in the numerical model. There are also a series of processes and boundary conditions that were not previously included in HydroGeoSphere explicitly. In the following section, the manner in which processes such as subglacial meltwater infiltration, permafrost formation and isostasy are explicitly included in the model is described.

5.1. Subglacial Meltwater Infiltration

[44] In some areas below the ice sheet, the basal ice is at the pressure melting point with resultant production of meltwater [*Paterson*, 1994]. As discussed in Section 4.1.2, basal meltwater, depending on the subglacial conditions, will either flow as recharge to the groundwater flow system or discharge over the land surface between the ice sheet sole and the rock surface.

[45] The proportion of subglacial meltwater that can recharge and subsequently be stored in the subsurface is undoubtedly uncertain and is a question of much debate in the literature because of its relevance to many issues regarding current water usage, sustainability and anthropogenic activity. There are several approaches that have been used to calculate recharge rates during glaciation. [*Breemer et al.*, 2002], for example, specified a constant flux equal to the subglacial meltwater rate, but obtained unrealistically high subsurface hydraulic heads in their model of the Michigan Lobe. They also examined a case having a high-permeability layer between the bedrock and the ice sheet. Only with the inclusion of a thin highly-permeable layer at the ice/bedrock interface, represented numerically by a highly transmissive fracture-type layer, could realistic subsurface heads be computed by the model. Therefore, the permeability of such a layer, and the spatiotemporal patterns of its permeability, becomes an issue on which little data exits that may be involved for verification. *McIntosh et al.* [2005] and *Forsberg* [1996] use a prescribed subsurface potentiometric head equal to the ice sheet thickness, expressed in terms of the equivalent freshwater head. This approach requires the assumption that the subglacial pressure never declines below the equivalent ice sheet weight, which has to be demonstrated. *Piotrowski* [1997a] also used a prescribed subsurface potentiometric head in his groundwater model at locations where the ice sheet covers the bedrock, but with the difference that it was inferred from paleoporewater pressures estimated from the stress characteristics of the fine-grained sediments overridden by the ice sheet [*Piotrowski and Kraus*, 1997]. According to these proxy estimates, the potentiometric surface was on average equal to 72% of the ice thickness. This approach seems to lead to realistic infiltration rates, but is restricted to the relatively small regions under study for which paleoporewater pressure data are available. Another approach was used by *Svensson* [1999], *Boulton et al.* [2001], and *Jaquet and Siegel* [2003, 2006] in which a specified meltwater rate is applied subglacially with the explicit inclusion of discrete subglacial tunnels (eskers) that will lower the water table because of their prescribed high hydraulic conductivity values. An arbitrary adjustment of the hydraulic conductivity of these tunnels can be made to achieve subglacial pressures slightly lower than the equivalent pressures induced by the ice sheet thickness to yield realistic infiltration rates. The major drawback of this approach is that the position, geometry and interconnectivity of the tunnels, and their hydraulic properties, must be known a priori; without this knowledge, it is clear that a stochastic, but geologically-constrained, probabilistic approach is needed.

[46] The modeling approaches mentioned above to couple glaciations to groundwater flow are based on a number of assumptions or process-related simplifications, that are especially required if they are to be applied at the scale of an entire basin or a continental land mass. Here, we use a mix of time-dependant boundary conditions that are more natural and less limited. For example, the manner in which subglacial meltwater enters the subsurface in the model is prescribed by a groundwater recharge flux that is dynamically constrained by the ice sheet thickness from one time step to the next. That is, a specified groundwater recharge flux equal to the predicted subglacial meltwater rate is applied to the subsurface only as long as the hydraulic head at the glacier's bed is lower than the ice equivalent freshwater head; otherwise the equivalent ice sheet head at any node in the computational grid and its difference with the groundwater head at the same location is used to control the subsurface subglacial infiltration. The ice equivalent freshwater head (L), h_{ice}, is given by $z_s + \rho_{ice} \cdot (z_{ice} - z_s)$, where $\rho_{ice} = 0.92$, is the relative density of ice (dimensionless), z_{ice} is the ice surface elevation (L) and z_s is the elevation of the land surface (L).

[47] The remainder of the meltwater is treated as direct overland runoff. The reasoning behind this treatment is that if the subsurface hydraulic head becomes higher than that equivalent to the ice sheet weight, the ice sheet would float and become unstable. The numerical solution results are analyzed after each time step and if any of the surficial grid nodes exhibit a head higher than the equivalent ice weight, the time step is restarted with a head specified as the ice weight for those nodes. This approach allows the computation of the fraction of meltwater that can naturally infiltrate into the subsurface, with the remainder assumed to participate in the surface runoff regime.

5.2. Permafrost Formation

[48] Permafrost develops where ground temperatures remain below the pressure melting point for over 2 consecutive years. In regions where permafrost forms, the relative permeability of the porous medium is greatly reduced. These regions are believed to exist at the ice sheet margins (e.g., *Hughes* [1998], *Boulton et al.* [1996], *Boulton and de Marsily* [1997], *King-Clayton et al.* [1995], *Cutler et al.* [2000], and *Tarasov and Peltier* [2007] among others). Permafrost forms because of very low temperatures and can propagate through the subsurface to depths as large as 1000 m or greater. Where the frozen ground is covered by an ice sheet, the temperature of the subsurface will tend to warm because the ice sheet will act as a blanket and isolate the ground from the extreme surface temperatures. The lateral extent of the permafrost zone therefore migrates along the ice sheet margins.

[49] Permafrost does not develop instantaneously; the freezing of water in the soil is instead a transient process. As water in the pores freezes, the permeability of the subsurface material to water is reduced and a relative permeability, as for unsaturated flow, can be defined as

$$k_{rw} = \frac{k(S_w)}{k_0}, \tag{29}$$

where k_{rw} is the relative permeability to water, k_0 is the permeability of the fully liquid-water saturated materials, and $k(S_w)$ is the permeability at liquid water saturation, S_w, with the remaining pore space filled with ice [*Kleinberg and Griffin*, 2005]. On account of capillary forces, water does not freeze completely and a thin film of liquid water covers the rock/soil grains even at low temperatures [*Kane and Stein*, 1983; *Gascoyne*, 2000; *Vidstrand*, 2003]; the amount of unfrozen water is directly related to the soil temperature and texture [*Kane et al.*, 2001] and more specifically the surface area of soil particles [*Anderson and Morgenstern*, 1973]. For this reason, neither S_w nor k_{rw} are allowed to reach zero.

[50] The hydraulic conductivity of permafrost is the product of the fully saturated hydraulic conductivity and the relative permeability to water: $K = K(S_w = 1)\, k_{rw}$. The water and ice saturations are not computed explicitly in HydroGeoSphere because frozen or unfrozen states are commonly obtained from permafrost depth calculations. For this reason, rather than specifying a permeability water saturation relationship, which is not well understood and for which little data are available, the hydraulic conductivity is simply allowed to vary between its frozen and unfrozen states. For the frozen state, a low hydraulic conductivity is specified (i.e., a 6 order of magnitude reduction) and, for the unfrozen state, the medium's default hydraulic conductivity value is used. Between these states, the permeability values are interpolated linearly between time steps so that they are progressively reduced or increased depending on the thermal regime. In order to include this progressive behavior in the model, time slices are selected (i.e., 1 ka), the finite elements located within the permafrost are selected and an interpolated low hydraulic conductivity value is assigned. If, for the next specified time slice an element is no longer affected by permafrost because of thawing, the assigned hydraulic conductivity value corresponds to a linear interpolation between the frost-free hydraulic conductivity value and the frozen value.

[51] Permafrost formation also has a significant impact on the geochemistry of groundwater because of a salt rejection phenomenon. When the water cools, the salt solubility in the water diminishes and two phenomena can occur: chemical precipitation or cryopeg formation [*Vidstrand*, 2003; *Vidstrand et al.*, 2006]. The cryopeg is a supercooled, saline liquid that forms in advance of the permafrost front as a consequence of salt rejection. This phenomenon is not included in the numerical model but the consequences will be discussed in the companion paper.

5.3. Isostasy

[52] Isostasy is the state of equilibrium between the Earth's crust and the mantle. The weight of the ice sheet will cause the Earth's crust to deform and a new state of equilibrium will prevail. The deformation of the crust by the ice sheet is such that the Earth's surface elevation will be depressed below the ice sheet and raised near its margins.

[53] The elevations of all the mesh nodes in each vertical grid column below the ice sheet are adjusted uniformly because the entire crust is depressed (or subsequently rebounds upon ice unloading). Since elevation changes from one time step to the next are relatively small compared to that which occurs over the entire glacial cycle, it is believed that this uniform coordinate adjustment of each vertical column of nodes will not produce significant fluid mass balance errors. On the other hand, the temporally and geographically changing elevation component of the hydraulic head will have a significant transient impact on groundwater flow patterns.

6. Summary

[54] Large-scale climate changes such as glaciations are suspected to have had a large impact on large groundwater flow systems such as sedimentary basins and continental environments. Recently, several studies, using environmental isotopes and salinity data, have suggested that significant subglacial meltwater may have infiltrated into the subsurface under the ambient ice sheet pressure and therefore become stored in the groundwater flow system. On account of the complexity and number of process involved, numerical models have become powerful tools to study the impact of glaciation on groundwater flow dynamics over large time frames.

[55] In this study, several key processes pertaining to continental-scale 3-D numerical modeling of groundwater flow during a glacial period were reviewed. These include subglacial infiltration, density-dependent (i.e., high-salinity) groundwater flow, permafrost evolution, isostasy, sea level changes and ice sheet loading. Traditional groundwater flow models are not adequate to model these phenomena, but appropriate assumptions and careful simplifications can be used to include them in existing numerical models with realism but with a minimum of modifications.

[56] One-dimensional hydromechanical coupling and brine generation were included in the numerical model HydroGeoSphere and tested against newly developed exact analytical solutions to verify their implementation. Verification examples were also used to explore the impact of subglacial boundary conditions on the surface/subsurface subglacial exchange flux. As observed by *Lemieux et al.* [2008a], meltwater infiltration into the subsurface dominates when the ice sheet is building up. Conversely, groundwater exfiltrates during ice sheet melting. Because of the high pressures at the bed of the ice sheet, meltwater is forced downward into the subsurface during ice sheet build-up and, when the ice sheet is melting, the pressure in the subsurface becomes higher than the basal meltwater pressure such that groundwater exfiltrates. This behavior, which is opposite to intuition, is a consequence of the interaction between the subglacial boundary conditions and the hydromechanical properties of the rocks, which is more clearly understood using a simple one-dimensional problem. A sensitivity analysis of the subglacial infiltration to the loading efficiency parameter was performed and showed that the infiltration rate into the subsurface diminishes with an increase of the loading efficiency parameter.

[57] In a companion paper [*Lemieux et al.*, 2008b], the model is applied to the Wisconsinian glaciation over the Canadian landscape in order to illustrate the concepts developed in this paper and to better understand the impact of glaciation on 3-D continental groundwater flow systems.

[58] **Acknowledgments.** Financial support for this study was provided by the Natural Sciences and Engineering Research Council of Canada (NSERC) and the Ontario Graduate Scholarship (OGS) Program as scholarships to J.-M. Lemieux and also from NSERC and the Canada Research Chairs program as research funding to E.A. Sudicky. The authors thank Grant Ferguson for carefully reviewing the three papers related to this work. We also appreciated the constructive reviews of Volker Rath, Mark Person, and the associate editor whose comments greatly helped to improve the original manuscript.

References

Adams, J. J., and S. Bachu (2002), Equations of state for basin geofluids: Algorithm review and intercomparison for brines, *Geofluids*, *2*, 257–271.

Anderson, D. M., and N. R. Morgenstern (1973), Physics, chemistry and mechanics of frozen ground: A review, in *Proceedings of 2nd International Conference on Permafrost, North American Contributions, Yakutsk, USSR*, pp. 257–288, Natl. Acad. of Sci., Washington, D. C.

Ates, Y., D. Bruneau, and W. R. Ridgway (1997), Continental glaciation and its possible impact on a used-fuel disposal vault in the Canadian Shield, *Tech. Rep. AECL-10140 COG-94-37-I*, At. Energy of Can. Ltd., Pinawa, Manit., Canada.

Bear, J. (1972), *Dynamics of Fluids in Porous Media*, Elsevier, New York.

Boulton, G. S., and G. de Marsily (1997), Hydrogeological aspects of glaciation, in *Glaciation and Hydrogeology, SKI Report 97:13*, edited by L. King-Clayton et al., pp. 33–44, Swed. Nucl. Power Insp., Stockholm.

Boulton, G. S., T. Slot, K. Blessing, P. Glasbergen, T. Leijnse, and K. van Gijssel (1993), Deep circulation of groundwater in overpressured subglacial aquifers and it's geological consequences, *Quat. Sci. Rev.*, *12*, 739–745.

Boulton, G. S., P. B. Caban, and K. van Gijssel (1995), Groundwater flow beneath ice sheets: Part I—Large scale patterns, *Quat. Sci. Rev.*, *14*, 545–562.

Boulton, G. S., P. B. Caban, K. van Gissel, A. Leijnse, M. Punkari, and F. H. A. van Weert (1996), The impact of glaciation on the groundwater regime of Northwest Europe, *Global Planet. Change*, *12*(1–4), 397–413.

Boulton, G. S., S. Zaptsepin, and B. Maillot (2001), Analysis of groundwater flow beneath ice sheets, *Tech. Rep. TR-01-06*, Swed. Nucl. Fuel and Waste Manage. Co., Stockholm.

Breemer, C. H., P. U. Clark, and R. Haggerty (2002), Modeling the subglacial hydrology of the late Pleistocene Lake Michigan Lobe, Laurentide Ice Sheet, *Geol. Soc. Am. Bull.*, *114*(6), 665–674.

Brouyère, S., G. Carabin, and A. Dassargues (2004), Climate change impacts on groundwater resources: Modelled deficits in a chalky aquifer, Geer basin, Belgium, *Hydrogeol. J.*, *12*(2), 123–134.

Burt, T. P., and P. J. Williams (1976), Hydraulic conductivity in frozen soils, *Earth Surf. Processes*, *1*(4), 349–360.

Carslaw, H. S., and J. C. Jaeger (1959), *Conduction of Heat in Solids*, 2nd ed., Oxford Univ. Press, New York.

Chan, T., and F. W. Stanchell (2005), Subsurface hydro-mechanical (HM) impacts of glaciation: Sensitivity to transient analysis, HM coupling, fracture zone connectivity and model dimensionality, *Int. J. Rock Mech. Min. Sci.*, *42*(5–6), 828–849.

Chan, T., R. Christiansson, G. S. Boulton, L. O. Ericsson, J. Hartikainen, M. R. Jensen, D. M. Ivars, F. W. Stanchell, P. Vistrand, and T. Wallroth (2005), DECOVALEX III BMT3/BENCHPAR WP4: The thermo-hydro-mechanical responses to a glacial cycle and their potential implications for deep geological disposal of nuclear fuel waste in a fractured crystalline rock mass, *Int. J. Rock Mech. Min. Sci.*, *42*(5–6), 805–827.

Clark, I. D., M. Douglas, K. Raven, and D. Bottomley (2000), Recharge and preservation of Laurentide glacial melt water in the Canadian Shield, *Ground Water*, *38*(5), 735–742.

Cutler, P. M., D. R. MacAyeal, D. Mickelson, B. R. Parizek, and P. M. Colgan (2000), A numerical investigation of ice-lobe-permafrost interaction around the southern Laurentide Ice Sheet, *J. Glaciol.*, *46*(153), 311–325.

de Hoog, F. R., J. R. Knight, and A. N. Stokes (1982), An improved method for numerical inversion of Laplace transforms, *SIAM J. Sci. Comput.*, *3*(3), 357–366.

Douglas, M., I. D. Clark, K. Raven, and D. Bottomley (2000), Groundwater mixing dynamics at a Canadian Shield mine, *J. Hydrol.*, *235*(1–2), 88–103.

Edmunds, W. M. (2001), Paleowaters in European coastal aquifers—The goals and main conclusions of the PALAEAUX project, *Geol. Soc. Spec. Publ.*, *189*, 1–16.

Ferguson, G. A. G., R. N. Betcher, and S. E. Grasby (2007), Hydrogeology of the Winnipeg Formation in Manitoba, Canada, *Hydrogeol. J.*, *15*, 573–587, doi:10.1007/s10040-006-0130-4.

Flowers, G. E., and G. K. C. Clarke (2002a), A multicomponent coupled model of glacier hydrology 1. Theory and synthetic examples, *J. Geophys. Res.*, *107*(B11), 2287, doi:10.1029/2001JB001122.

Flowers, G. E., and G. K. C. Clarke (2002b), A multicomponent coupled model of glacier hydrology 2. Application to Trapridge Glacier, Yukon, Canada, *J. Geophys. Res.*, *107*(B11), 2288, doi:10.1029/2001JB001124.

Forsberg, C. F. (1996), Possible consequences of glacially induced groundwater flow, *Global Planet. Change*, *12*(1–4), 387–396.

Freeze, A., and J. A. Cherry (1979), *Groundwater*, Prentice-Hall, Upper Saddle River, N. J.

Frind, E. O. (1982), Simulation of long-term transient density-dependant transport in groundwater, *Adv. Water Resour.*, *5*(2), 73–88.

Gascoyne, M. (2000), A review of published literature on the effects of permafrost on the hydrogeochemistry of bedrock, *Posiva Rep. 2000-09*, Posiva Oy, Helsinki.

Graf, T. (2005), Modeling coupled thermohaline flow and reactive solute transport in discretely-fractured porous media, Ph.D. thesis, Université Laval, Québec City, Qué., Canada.

Grasby, S., K. Osadetz, R. Betcher, and F. Render (2000), Reversal of the regional-scale flow system of the Williston basin in response to Pleistocene glaciation, *Geology*, *28*(7), 635–638.

Grasby, S. E., and Z. Chen (2005), Subglacial recharge into the western Canada sedimentary basin—Impact of Pleistocene glaciation on basin hydrodynamics, *Geol. Soc. Am. Bull.*, *117*(3–4), 500–514.

Heathcote, J. A., and U. M. Michie (2004), Estimating hydrogeological conditions over the last 120 ka: an example from the Sellafield area, UK, *J. Geol. Soc. London*, *161*, 995–1008.

Hoaglund, J. R., III, J. J. Kolak, D. T. Long, and G. J. Larson (2004), Analysis of modern and Pleistocene hydrologic exchange between Saginaw Bay (Lake Huron) and the Saginaw Lowlands area, *Geol. Soc. Am. Bull.*, *116*(1–2), 3–15.

Hughes, T. J. (1998), *Ice Sheets*, 343 pp., Oxford Univ. Press, Oxford, U. K.

International Permafrost Association Standing Committee on Data Information and Communication (2003), Circumpolar active-layer permafrost system [CD-ROM], version 2.0, edited by M. Parsons and T. Zhang, Natl. Snow and Ice Data Cent./World Data Cent. for Glaciol., Boulder, Colo.

Jaquet, O., and P. Siegel (2003), Groundwater flow and transport modelling during a glaciation period, *Tech. Rep. TR-03-04*, Swed. Nucl. Fuel and Waste Manage. Co., Stockholm.

Jaquet, O., and P. Siegel (2006), Regional groundwater flow model for a glaciation scenario: Simpevarp subarea—Version 1.2, *Tech. Rep. TR-06-100*, Swed. Nucl. Fuel and Waste Manage. Co., Stockholm.

Kane, D. L., and J. Stein (1983), Water movement into seasonally frozen soils, *Water Resour. Res.*, *19*(6), 1547–1557.

Kane, D. L., K. M. Hinkel, D. J. Goering, L. D. Hinzman, and S. I. Outcalt (2001), Non-conductive heat transfer associated with frozen soils, *Global Planet. Change*, *29*, 275–292.

King-Clayton, L. M., N. A. Chapman, F. Kautsky, N.-O. Svensson, G. de Marsily, and E. Ledoux (1995), The central scenario for SITE-94: A climate change scenario, *SKI Rep. 95:42*, Swed. Nucl. Power Insp., Stockholm.

Kleinberg, R. L., and D. D. Griffin (2005), NMR measurements of permafrost: Unfrozen water assay, pore-scale distribution of ice, and hydraulic permeability of sediments, *Cold Reg. Sci. Technol.*, *42*(1), 63–77.

Lemieux, J.-M. (2006), Impact of the Wisconsinian glaciation on Canadian continental groundwater flow, Ph.D. thesis, University of Waterloo, Waterloo, Ont., Canada.

Lemieux, J.-M., E. A. Sudicky, W. R. Peltier, and L. Tarasov (2008a), Dynamics of groundwater recharge and seepage over the Canadian landscape during the Wisconsinian glaciation, *J. Geophys. Res.*, *113*, F01011, doi:10.1029/2007JF000838.

Lemieux, J.-M., E. A. Sudicky, W. R. Peltier, and L. Tarasov (2008b), Simulating the impact of glaciations on continental groundwater flow systems: 2. Model application to the Wisconsinian glaciation over the Canadian landscape, *J. Geophys. Res.*, doi:10.1029/2007JF000929, in press.

McEwen, T., and G. de Marsily (1991), The potential significance of premafrost to the behaviour of a deep radioactive waste repository, *SKI Rep. 91:8*, Swed. Nucl. Power Insp., Stockholm.

McIntosh, J. C., and L. M. Walter (2005), Volumetrically significant recharge of Pleistocene glacial meltwaters into epicratonic basins:

Constraints imposed by solute mass balances, *Chem. Geol.*, *222*(3–4), 292–309.
McIntosh, J. C., L. M. Walter, and A. M. Martini (2002), Pleistocene recharge to midcontinent basins: Effects on salinity structure and microbial gas generation, *Geochim. Cosmochim. Acta*, *66*(10), 1681–1700.
McIntosh, J. C., G. Garven, and J. S. Hanor (2005), Modeling variable-density fluid flow and solute transport in glaciated sedimentary basins, *Eos Trans. AGU*, *86*(52), Fall Meet. Suppl., Abstract H11D-1310.
McKenzie, J. M., C. I. Voss, and D. I. Siegel (2007), Groundwater flow with energy transport and water-ice phase change: Numerical simulations, benchmarks, and application to freezing in peat bogs, *Adv. Water Resour.*, *30*(4), 966–983.
Neuzil, C. E. (2003), Hydromechanical coupling in geological processes, *Hydrogeol. J.*, *11*(1), 41–83.
Paterson, W. S. B. (1994), *The Physics of Glaciers*, 3rd ed., 480 pp., Pergamon, Oxford, U. K.
Peltier, W. R. (1994), Ice age paleotopography, *Science*, *265*, 195–201.
Person, M., B. Dugan, J. B. Swenson, L. Urbano, C. Stott, J. Taylor, and M. Willett (2003), Pleistocene hydrogeology of the Atlantic continental shelf, New England, *Geol. Soc. Am. Bull.*, *115*(11), 1324–1343.
Person, M., J. McIntosh, V. Bense, and V. H. Remenda (2007), Pleistocene hydrology of North America: The role of ice sheets in reorganizing groundwater flow systems, *Rev. Geophys.*, *45*, RG3007, doi:10.1029/2006RG000206.
Piotrowski, J. A. (1997a), Subglacial groundwater flow during the last glaciation in northwestern Germany, *Sediment. Geol.*, *111*, 217–224.
Piotrowski, J. A. (1997b), Subglacial hydrology in north-western Germany during the last glaciation: Groundwater flow, tunnel, valleys and hydrological cycles, *Quat. Sci. Rev.*, *16*, 169–185.
Piotrowski, J. A., and A. Kraus (1997), Response of sediment to ice sheet loading in northwestern Germany: Effective stresses and glacier bed stability, *J. Glaciol.*, *43*(145), 495–502.
Provost, A. M., C. I. Voss, and C. E. Neuzil (1998), Glaciation and regional ground-water flow in the Fennoscandian shield; Site 94, *SKI Rep. 96:11*, Swed. Nucl. Power Insp., Stockholm.
Raven, K. G., D. J. Bottomley, R. A. Sweezey, J. A. Smedley, and T. J. Ruttan (1987), Hydrogeological characterization of the East Bull Lake research area, *Natl. Hydrol. Res. Inst. Pap. 31/Inland Waters Dir. Ser. 160*, Environ. Canada, Ottawa, Ont.
Sheppard, M. I., B. D. Amiro, P. A. Davis, and D. R. Zach (1995), Continental glaciation and nuclear fuel waste disposal: Canada's approach and assessment of the impact on nuclide transport through the biosphere, *Ecol. Model.*, *78*(3), 249–265.
Siegel, D. I. (1989), Geochemistry of the Cambrian-Ordovician aquifer system in the northern midwest, United States, *U.S. Geol. Surv. Prof. Pap. 1405-D*, U.S. Geol. Surv., Denver, Colo.
Siegel, D. I. (1991), Evidence for dilution of deep, confined ground water by vertical recharge of isotopically heavy Pleistocene water, *Geology*, *19*(5), 433–436.
Siegel, D. I., and R. J. Mandle (1983), Isotopic evidence for glacial meltwater recharge to the Cambrian-Ordovician aquifer, north-central United States, *Quat. Res.*, *22*(3), 328–335.
Smith, S. L., and M. M. Burgess (2002), A digital database of permafrost thickness in Canada, *Geol. Surv. Can. Open File 4173*, Geol. Surv. of Can., Ottawa, Ont.
Svensson, U. (1999), Subglacial groundwater flow at Äspö as governed by basal melting and ice tunnels, *Tech. Rep. TR-99-38*, Swed. Nucl. Fuel and Waste Manage. Co., Stockholm.
Talbot, C. J. (1999), Ice ages and nuclear waste isolation, *Eng. Geol.*, *52*(3–4), 177–192.
Tarasov, L., and W. R. Peltier (1999), Impact of thermomechanical ice sheet coupling on a model of the 100 kyr ice age cycle, *J. Geophys. Res.*, *104*(D8), 9517–9545.
Tarasov, L., and W. R. Peltier (2002), Greenland glacial history and local geodynamic consequences, *Geophy. J. Int.*, *150*, 198–229.
Tarasov, L., and W. R. Peltier (2004), A geophysically constrained large ensemble analysis of the deglacial history of the North American ice-sheet complex, *Quat. Sci. Rev.*, *23*(3–4), 359–388.
Tarasov, L., and W. R. Peltier (2006), A calibrated deglacial drainage chronology for the North American continent: Evidence of an Arctic trigger for the Younger Dryas, *Quat. Sci. Rev.*, *25*(7–8), 659–688.
Tarasov, L., and W. R. Peltier (2007), Coevolution of continental ice cover and permafrost extent over the last glacial-interglacial cycle in North America, *J. Geophys. Res.*, *112*, F02S08, doi:10.1029/2006JF000661.
Teller, J. T. (1987), Proglacial lakes and the southern margin of the Laurentide Ice Sheet, in *North America and Adjacent Oceans During the Last Deglaciation*, edited by W. F. Ruddiman and H. E. Wright, pp. 39–67, Geol. Soc. of Am., Boulder, Colo.
Teller, J. T. (1990), Volume and routing of late-glacial runoff from the southern Laurentide Ice Sheet, *Quat. Res.*, *34*(1), 12–23.
Therrien, R., and E. A. Sudicky (1996), Three-dimensional analysis of variably-saturated flow and solute transport in discretely-fractured porous media, *J. Contam. Hydrol.*, *23*(1–2), 1–44.
Therrien, R., R. McLaren, E. A. Sudicky, and S. Panday (2006), *HydroGeoSphere—A Three-Dimensional Numerical Model Describing Fully-Integrated Subsurface and Surface Flow and Solute Transport*, Groundwater Simul. Group, Waterloo, Ont., Canada.
van Weert, F. H. A., K. van Gijssel, A. Leijnse, and G. S. Boulton (1997), The effects of Pleistocene glaciations on the geohydrological system of Northwest Europe, *J. Hydrol.*, *195*(1–4), 137–159.
Vidstrand, P. (2003), Surface and subsurface conditions in permafrost areas—A literature review, *Tech. Rep. TR-03-06*, Swed. Nucl. Fuel and Waste Manage. Co., Stockholm.
Vidstrand, P., U. Svensson, and S. Follin (2006), Simulation of hydrodynamic effects of salt rejection due to permafrost—Hydrogeological numerical model of density-driven mixing, at a regional scale, due to a high salinity pulse, *Tech. Rep. R-06-101*, Swed. Nucl. Fuel and Waste Manage. Co., Stockholm.
Wang, H. F. (2000), *Theory of Linear Poroelasticity With Applications to Geomechanics and Hydrogeology*, 287 pp., Princeton Univ. Press, Princeton, N. J.
Weaver, T. R., S. K. Frape, and J. A. Cherry (1995), Recent cross-formational fluid flow and mixing in the shallow Michigan Basin, *Geol. Soc. Am. Bull.*, *107*(6), 697–707.

J.-M. Lemieux and E. A. Sudicky, Department of Earth and Environmental Sciences, University of Waterloo, Waterloo, ON, Canada N2L 3G1. (jmlemieux@alumni.uwaterloo.ca; sudicky@sciborg.uwaterloo.ca)

W. R. Peltier, University of Toronto, Department of Physics, 60 St. George Street, Toronto, ON, Canada M5S 1A7. (peltier@atmosp.physics.utoronto.ca)

L. Tarasov, Department of Physics and Physical Oceanography, Memorial University of Newfoundland, St. John's, NL, Canada A1C 5S7. (lev@physics.mun.ca)